to the integrals

$$\mathcal{E}_{0\xi} \cong -(\mathcal{E}_{0\xi})^2; \tag{D3}$$

consequently, the numerator and denominator of (D1) are equal in the limit, giving

$$dc/df = 1. \tag{D4}$$

On the other hand, for the isolated accumulation layer $c_1 \to 0$. This follows directly from (C13) inasmuch as in the boundary

$$\mathcal{E}_{0\xi} \underset{\eta \to 0}{\to} (1/\eta)u(\mathcal{E}_0), \tag{D5}$$

which becomes indefinitely large as the thickness decreases. The numerator varies as η^{-1} and the denominator as η^{-2}. Therefore $c_1 \sim O(\eta)$ which vanishes in this limit of $\eta \to 0$, giving

$$dc/df = 0. \tag{D6}$$

The conclusion is that in the limit of slight diffusion, the depletion layer has a velocity

$$c = f = v(\mathcal{E}_a), \tag{D7}$$

while the velocity of the accumulation layer is the constant

$$c = f_c, \tag{D8}$$

independent of f.

PHYSICAL REVIEW VOLUME 155, NUMBER 2 10 MARCH 1967

Nature of the ac Transition in the Superconducting Surface Sheath in Pb-2% In

R. W. ROLLINS* AND J. SILCOX

Department of Engineering Physics and Laboratory of Atomic and Solid State Physics, Cornell University, Ithaca, New York

(Received 24 August 1966)

The response of the superconducting sheath state of Pb–2wt% In to low-frequency (20–500 cps), small-amplitude (10^{-2} Oe $< h_0 <$ 20 Oe) ac fields has been studied. Direct observation of the wave form shows that screening currents are developed in the sheath up to a critical value J_c, when the field begins to penetrate. The screening current continues to increase until a saturation value J_s is reached, at which point the current in the sheath stays constant for the remainder of the half-cycle. Fourier analysis of a model wave form for which $J_m = J_c = J_s$ indicates the harmonic content, and nonlinear nature, of the response. Measurements of the real and imaginary parts of the ac permeability, μ' and μ'', at the fundamental frequency as a function of the ac field amplitude at constant dc field shows that the transition is characterized by only one parameter, dependent on the dc field, and that the model gives an excellent description of the nonlinearity. Well-defined quantitative critical-current data can be obtained for comparison with the theories of Abrikosov, Park, and Fink and Barnes. The relationship between these observations and other measurements of μ' and μ'' as a function of dc field at constant ac field amplitude is discussed. It is shown that the transition is sensitive to misalignment of the specimen relative to the dc field. The change in the transition as the frequency is changed is explored, and a preliminary conclusion is that J_s is much more sensitive to frequency than J_c.

1. INTRODUCTION

SUPERCONDUCTORS have been studied by ac magnetic field techniques for a considerable time.[1] We are concerned in this paper with experiments of the type[2] in which a small axial ac magnetic field $h(t) = h_0 \cos\omega t$ with a frequency in the range 20 cps $< \omega <$ 500 cps is superimposed upon a coaxial dc field H_0. If H_0 is in the range $H_{c2} < H_0 < H_{c3}$ for a type-II superconductor, or in the range $H_c < H_0 < H_{c3}$ for an appropriate type-I superconductor, the specimen is in the superconducting sheath state discussed by St. James and de Gennes[3] and experimentally confirmed by various investigators.[4,5] The response of a specimen in this regime to such an ac field probe has in the past been measured in the form of the in- and out-of-phase permeability components μ' and μ'' as a function of the dc field H_0 at constant ac field amplitude h_0 and at the fundamental frequency. Characteristic features[5–10] of the response

* Present address: Ohio University, Athens, Ohio.

[1] D. Shoenberg, Proc. Cambridge Phil. Soc. **33**, 559 (1937).

[2] See, e.g., R. A. Hein and R. L. Falge, Jr., Phys. Rev. **123**, 407 (1961).

[3] D. St. James and P. G. De Gennes, Phys. Letters **7**, 306 (1963).

[4] C. F. Hempstead and Y. B. Kim, Phys. Rev. Letters **12**, 145 (1964); W. J. Tomasch and A. S. Joseph, *ibid.* **12**, 148 (1964); G. Bon Mardion, B. B. Goodman, and A. Lacaze, Phys. Letters **8**, 15 (1964); S. Gygax, J. L. Olsen, and R. H. Kropschot, *ibid.* **8**, 228 (1964); M. Cardona and B. Rosenblum, *ibid.* **8**, 308 (1964); B. Rosenblum and M. Cardona, *ibid.* **8**, 220 (1964); J. P. Burger, G. Deutscher, E. Guyon and A. Martinet, Solid State Commun. **2**, 101 (1964).

[5] M. Strongin, A. Paskin, D. G. Schweitzer, O. F. Kammerer, and P. P. Craig, Phys. Rev. Letters **12**, 442 (1964).

[6] E. Maxwell and M. Strongin, Phys. Rev. Letters **10**, 212 (1963).

[7] M. Strongin and E. Maxwell, Phys. Letters **6**, 49 (1963).

[8] P. R. Doidge and Kwan Sik-Hung, Phys. Letters **12**, 82 (1964).

[9] P. P. J. Van Engelen, G. J. C. Bots, and B. S. Blaisse, Phys. Letters **19**, 465 (1965).

[10] R. W. Rollins and J. Silcox, in Proceedings of the Conference on the Physics of Type-II Superconductivity, Western Reserve University, 1964, p. III-32 (unpublished).

include discontinuities in the slopes of both $\mu'(H_0)$ and $\mu''(H_0)$ at H_{c2}, normal-state values of μ' and μ'' at H_{c3} for "good" samples, an intermediate peak in μ'', and nonlinear response with respect to h_0, even though $h_0/H_0 \approx 10^{-3}$ or less. In the superconducting state, μ'' is very much higher than in the normal state, implying[11] that much more power is dissipated in the specimen in the sheath state.

Maxwell and Strongin[6] first drew attention to the similarity of these results to those predicted for a normal metal as the ratio of the normal skin depth to diameter changes from 0 to ∞. Following the work of St. James and de Gennes, superconductivity in this high-field region was recognized to be confined to within about a coherence length of the surface. Thus, further models (based upon the normal resistivity analogy) assigned to the surface layer of thickness d, a conductivity σ, which is different from the normal conductivity of the bulk σ_n.[8,12] The conductivity of the surface layer is then considered to be a function of the applied dc field going to the normal-state value at $H_0 \geq H_{c3}$. This model has been shown to result in a peak in μ'' and is in qualitative agreement with measurements of μ' and μ'' as a function of the dc field in the superconducting-sheath region, while the ac field amplitude is kept constant. In fact, the quantitative fit to the position and height of the peak in μ'' is fairly good, and the apparent successes of this type of model suggested that its interpretation might be pushed further. Thus, because of the difference between the predicted height and location of the peak in μ'' for the bulk effective-conductivity and surface effective-conductivity models, it was suggested[8,12] that perhaps careful measurements of μ' and μ'' for a superconductor with $H_0 > H_{c2}$ would make possible a determination of whether the losses in this case are due to a surface or a bulk effect. We note, however, that these models, taken at face value, are linear in h_0, in contradiction to experiment.

We report here in detail experiments which show that, despite the above-mentioned successes of the effective-conductivity model, it does not give an adequate description of the wave form corresponding to the flux passing through the specimen. This leads directly to a model comparable to one discussed qualitatively by Paskin *et al.*[13] and more quantitatively by Fink[14] and consistent with observations of the dc magnetization.[15] The approach is similar to that used by Bean in his use of ac techniques to determine critical currents in synthetic filamentary superconductors[16] and hysteretic type-II superconductors[17] for $H_0 < H_{c2}$. The observations show that under certain conditions, i.e., careful surface preparation and very low frequency ac fields, well-defined quantitative experimental information can be obtained to be compared with the theoretical predictions of Abrikosov,[18] Park,[19,20] and Fink and Barnes,[21] for the critical magnetization of the surface sheath in the critical state. It is shown that measurements of μ' and μ'' taken as a function of h_0 at constant H_0 afford a much more sensitive test of the various models than the previous measurements. Finally, by observing the wave form directly, one can study the transitions in the surface sheath when conditions are not ideal. A brief account of similar work on a Pb–8 wt% In alloy has been published elsewhere.[22]

2. THEORETICAL BACKGROUND

During the course of theoretical and experimental work on the sheath state, it has become apparent that the sheath is capable of supporting lossless currents up to a critical value. Abrikosov,[18] and later Park,[19] minimized the Ginzburg-Landau (G-L) expression[23] for the total free energy at a constant applied field H_0, over the manifold of functions ψ, the order parameter, and A, the vector potential, which lead to a state with a given net current and which satisfy the boundary conditions appropriate for the surface-sheath state. The critical current at a given H_0 is then defined as the maximum given current for which a function ψ can be found from the minimization process. Fink and Barnes[21] point out that if currents are induced in a multiply connected superconducting sheath, as in the present experiments, then the contribution to the free energy from the shielded magnetic field is relatively large. The free energy in the current-carrying states described by Abrikosov very quickly becomes much larger than the normal-state free energy. Since the superconducting state may well be unstable with respect to the normal state in these circumstances, Fink and Barnes[21] suggest that the approproate criterion that determines the critical current may be that the free-energy difference between the superconducting and normal states be zero. Values obtained in this way are considerably lower than those given by Abrikosov and Park. Park[20] has also

[11] See, e.g., L. D. Landau and E. M. Lifshitz, *Electrodynamics of Continuous Media* (Pergamon Press, Inc., New York, 1960), p. 192.
[12] A. Paskin, M. Strongin, P. P. Craig, and D. G. Schweitzer, Phys. Rev. **137**, A1816 (1965).
[13] A. Paskin, M. Strongin, D. G. Schweitzer, and B. Bertman, Phys. Letters **19**, 277 (1965).
[14] H. J. Fink, Phys. Rev. Letters **16**, 447 (1966).
[15] C. Chiou, R. A. Connell, and D. P. Seraphim, Phys. Rev. **129**, 1070 (1963); D. J. Sandiford and D. G. Schweitzer, Phys. Letters **13**, 98 (1964); L. J. Barnes and H. J. Fink, *ibid.* **20**, 583 (1966); D. P. Jones and J. G. Park, *ibid.* **20**, 111 (1966).
[16] C. P. Bean, Rev. Mod. Phys. **36**, 31 (1964).
[17] C. P. Bean, R. L. Fleischer, P. S. Swartz, and H. R. Hart, Jr., J. Appl. Phys. **37**, 2218 (1966).
[18] A. A. Abrikosov, Zh. Eksperim. i Teor. Fiz. **47**, 720 (1964) [English transl.: Soviet Phys.—JETP **20**, 480 (1965)].
[19] J. G. Park, Phys. Rev. Letters **15**, 352 (1965).
[20] J. G. Park, Phys. Rev. Letters **16**, 1196 (1966).
[21] H. J. Fink and L. J. Barnes, Phys. Rev. Letters **15**, 793 (1965).
[22] R. W. Rollins and J. Silcox, Solid State Commun. **4**, 323 (1966).
[23] V. L. Ginzburg and L. D. Landau, Zh. Eksperim. i Teor. Fiz. **20**, 1964 (1950) [English transl. in D. Ter Haar, *Men of Physics: L. D. Landau* (Pergamon Press, Inc., New York, 1965), p. 138].

refined the Fink and Barnes estimates. Both types of calculation have been one dimensional.

A simple view of the situation can be obtained in the following way. We are primarily interested in the response of a long cylindrical specimen with the applied field along the axis of the cylinder. In this case, it is reasonable to assume cylindrical symmetry with the z axis along the applied field. Then $\psi=F_n(\rho)e^{in\theta}$, where n must be an integer because of the usual single-valued condition on ψ, and θ and ρ are cylindrical coordinates. The G-L free energy now depends on the functions $F_n(\rho)$ and $A_n(\rho)$ and the parameter n. Minimizing this total free energy at fixed H_a and n with respect to variations in the functions $F_n(\rho)$ and $A_n(\rho)$ results in a set of G-L equations to be satisfied by $F_n(\rho)$ and $A_n(\rho)$ for each n. Thus, for any given value of the applied field there are many superconducting states available which correspond to local minima in the total free energy, each state with label n. Three such states are illustrated schematically in Fig. 1. The stable equilibrium state will be that state which gives the lowest value of the total free energy; all states corresponding to other n values will be metastable or unstable at that applied field. Thus, in Fig. 1, at a field H_a the lowest state will be that labeled n and the states $n-1$ and $n+1$ will be metastable. It is easy to show that minimization of the total free energy with respect to the various n values leads to the condition that the net circulating current be zero, or very nearly zero, as demonstrated by St. James and de Gennes[3] and also Abrikosov[18] for the sheath state. This implies that the field in the bulk when the sheath is in the lowest free-energy state is equal to the applied field H_a.

From the definition of flux and the second G-L equation, one obtains the G-L equivalent of the London fluxoid quantization[24] condition

$$\Phi(\rho)+2\pi\rho\left[\frac{|\psi_0|^2}{F_n^2(\rho)}\frac{4\pi}{c}\lambda^2\right]j(\rho)=n\varphi_0, \qquad (1)$$

where $\Phi(\rho)$ is the total flux passing within radius ρ, $j(\rho)$ is the current density in the θ direction at radius ρ, λ is the weak-field penetration depth of the G-L theory, $|\psi_0|$ is the amplitude of order parameter in zero applied field, and φ_0 is the usual fluxoid quantum.[24] The current density of the stable equilibrium sheath is known to pass through zero very close to the surface. Applying Eq. (1) at the radius at which this occurs shows the total flux within that radius to be $n\varphi_0$. Thus, the lowest equilibrium state corresponds to $n\approx\pi R^2H_a/\varphi_0$, to order ξ/R, where ξ is the coherence distance and R is the radius of the sample. The radius at which $j(\rho)=0$ will shrink for a net diamagnetic current and increase for a net paramagnetic current.[19] For states carrying a net surface current which is small compared to the currents already present in the stable equilibrium sheath, it is reasonable to assume that this change will be insignificant. Experiments show that the resulting critical current is much smaller than the currents already present in the surface state, as calculated by Fink and Kessinger.[25] Thus, applying Eq. (1) again shows that the internal field of the nth state is given by $B_n=n\varphi_0/\pi R^2$, again to order ξ/R, and is independent of the applied field as long as $|H_a-B_n|$ is not too large.

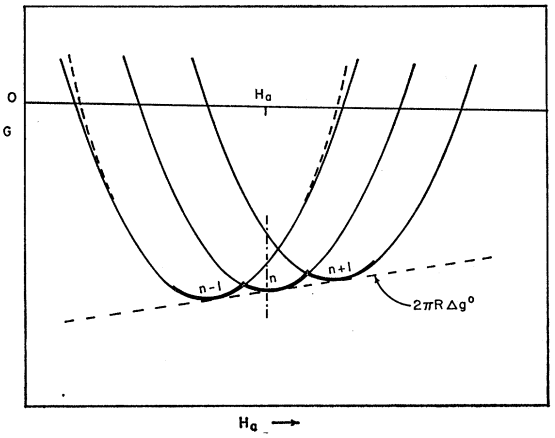

FIG. 1. A schematic illustration of the free-energy parabolas corresponding to integer n. In practice, the parabolas are very much closer together. The modification to the parabolic form as calculated by Park (Ref. 20) is schematically shown as the dashed line. At an applied field H_a, the lowest state n is slightly paramagnetic, $n+1$ is paramagnetic, and $n-1$ is diamagnetic.

Since the functions $F_n(\rho)$ and $A_n(\rho)$ are solutions of the G-L equations, the free-energy difference between the superconducting state and the normal state may be written as

$$\Delta G_n=\int dV\left[\frac{(H_a-B_i)^2}{8\pi}-\frac{H_c^2}{8\pi}\frac{|F_n(\rho)|^4}{|\psi_0|^4}\right], \qquad (2)$$

where H_c is the thermodynamic critical field and B_i is the internal field which tends to B_n in the bulk. For $H_a=B_n$, the contribution to the free energy proportional to the area disappears and we may put $\Delta G_n^0=2\pi R\Delta g_n^0$ per unit length of sample where Δg_n^0 is now a surface free-energy difference. H_{c3} is given by $\Delta g_n^0=0$. We expect Δg_n^0 to be affected only slightly by the addition of a net surface current much smaller than the currents present in the sheath. Under these conditions, the total free energy of the nth state relative to the normal state is given by

$$\Delta G_n=(\pi R^2/8\pi)(H_a-B_n)^2-2\pi R\Delta g_n^0. \qquad (3)$$

Referring to Fig. 1, we see that at an applied field H_a, the internal fields corresponding, respectively, to the states $n-1$, n, and $n+1$ are equal to the field values at the minima of the corresponding free-energy wells.

[24] F. London, *Superfluids* (Dover Publications, Inc., New York, 1960), p. 152.

[25] H. J. Fink and R. D. Kessinger, Phys. Rev. **140**, A1937 (1965).

Thus, the metastable states $n-1$, and $n+1$ correspond, respectively, to diamagnetic and paramagnetic states.

If the surface sheath was to stay in stable equilibrium as the applied field is changed, the path followed would be the heavy scalloped curve with cusps shown in Fig. 1. The resulting net currents developed when the system is at a cusp would be negligible. For example, for $R\sim 1$ mm the change in field corresponding to $\Delta n=1$ is $\varphi_0/\pi R^2\approx 10^{-5}$ Oe. However, experiments show that the surface sheath is capable of shielding fields of the order of 1 Oe or more. Thus, the sheath must be unable to make the transition from one n value to another when these states first reach thermodynamic equilibrium. In order to make this unlikely transition, the supercurrents would have to reverse polarity. Instead, the sheath remains in a state of given n well after changes in the applied field have made the state metastable. The sheath continues to ignore changes in the applied field until, for some reason, it is able to make the transition from the metastable state to either another superconducting sheath state corresponding to a different n, or perhaps to the normal state. The point at which this transition occurs determines the critical surface current J_c or the critical change in field h_c which the surface sheath can endure without transition.

As mentioned previously, Fink and Barnes assume the transition occurs when the metastable state comes into equilibrium with the normal state while Abrikosov assumes that the transition does not occur until the solutions of the G-L equations corresponding to the metastable state cease to exist. Neither approach may be used to determine the final state after the transition. However, dc magnetization measurements[15] showing the effect of the surface sheath, along with ac measurements like those reported here, show that the transition is not to the normal state, but rather that the final state is another metastable superconducting sheath state with Δn relatively small.

The values for the critical current predicted by Fink and Barnes can be obtained readily from Eq. (3) by setting $\Delta G_n=0$. Ignoring the magnetic contribution to the surface free energy, $\Delta g_n{}^0$ can be written in the form $(H_c{}^2/8\pi)\Delta_n'[F_n(R)/\psi_0]^4$, where Δ_n' is approximately $\int_0{}^R F_n{}^4(\rho)d\rho/F_n{}^4(R)$. Thus,

$$\frac{4\pi}{c}J_c=h_c=H_c\left(\frac{2\Delta_n'}{R}\right)^{1/2}\left|\frac{F(R)}{\psi_0}\right|^2. \tag{4}$$

Written in the notation used by Fink and Barnes, we have essentially their result

$$\frac{4\pi J_c}{c}=(\beta)^{1/2}\frac{H_c}{\kappa}\left(\frac{2\lambda}{R}\right)^{1/2}\frac{\Delta}{\xi}F^2(R), \tag{5}$$

where $\kappa=\lambda/\xi$. The quantity $(\Delta/\xi)F^2(R)$ as a function of H_0/H_{c2} may be obtained from the results of Fink and Kessinger[25] and, for $\kappa\geq 3$, ranges from 0.038 at $H_0/H_{c2}=1.6$ to 0.74 at $H_0/H_{c2}=1.0$. The same treatment may be applied to a flat strip of width w and thickness t with the field applied along the length of the slab. The result is

$$h_c=H_c\left(\frac{2\Delta'(w+t)}{wt}\right)^{1/2}\frac{|\psi(R)|^2}{|\psi_0|^2},$$

which reduces to the previous result with R replaced by t if $w\gg t$. For a typical size specimen $2\lambda/R\approx 10^{-3}$ to 10^{-4} and taking $\beta\approx 1$ (following Fink and Barnes) we find that the values of Fink and Barnes for J_c are less than the Park[19] values by roughly a factor of 10. Park[20] has recently reported different values obtained from computer calculations using the same criteria as Fink and Barnes.

3. EXPERIMENTAL TECHNIQUES

A. Magnetization Measurements

The experimental apparatus is shown in Fig. 2. The dc field is supplied by a Magnion iron-cored magnet with field uniformity over the specimen better than 1 part in 10^4 and stability about 1 part in 10^6, as measured by nuclear-magnetic-resonance techniques. The dc field is measured and controlled by a Magnion FFC-4 field-control unit. The ac field is supplied by two identical drive coils about 57-mm long with an inner diameter of 5 mm and consisting of two layers (approximately 385

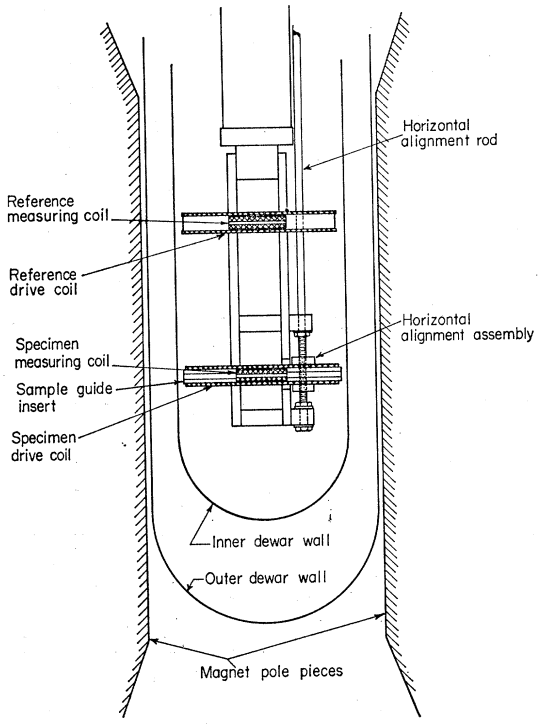

FIG. 2. Experimental arrangement in the Dewar.

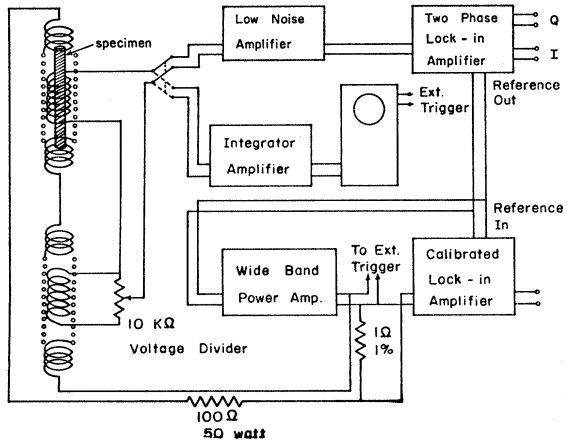

FIG. 3. Block diagram of electronic circuitry.

turns) of #30 wire held rigid by epoxy resin. The drive coils are connected in series with one coil providing an in-phase reference field and the other supplying the ac field for the specimen. Located in the center of the reference drive coil is a detection coil about 23 mm long and containing 7000 turns of #43 copper wire. The specimen detection coil is 21 mm long and contains 6000 turns of #43 wire. The pickup coil and specimen-guide insert slip snugly inside the specimen drive coil. A length of threaded rod attached to one end of the drive coil containing the specimen allows it to be tilted while immersed in liquid helium by turning the alignment rod. This, together with rotation of the iron magnet, allows precise alignment of the specimen with the dc field by maximizing the critical shielding current of the surface sheath at a fixed dc field.

A block diagram of the electronic circuit is shown in Fig. 3. The drive coils, connected in series with a 100-Ω, 50-W, load resistor and a 1-Ω precision resistor, are driven by a Krohn-Hite model DC-50-A wide-band power amplifier. A sine wave form has been used at frequencies of 20 to 500 cps generated by a Princeton Applied Research model JB-6 lock-in amplifier operating in the internal mode. This drive system can supply ac fields to the specimen ranging in amplitude from zero to about 100 Oe. The amplitude of the ac field is monitored as the voltage drop across the precision (~1%) 1-Ω resistor using a Princeton Applied Research calibrated lock-in amplifier model HR-8. The absolute determination of the ac field amplitude by this method is accurate to within 5%, the major error being in the geometrical factor for the drive coils. For some measurements, the x axis of an Electronic Associates Inc. 1110 x-y recorder is energized by the recorder output of the HR-8.

The voltage developed in the detection coil containing the specimen represents the flux passing through the specimen plus the flux passing through the free space between the specimen and the windings of the pickup coil. The latter excess voltage is cancelled off using the signal from the reference pickup coil and a General Radio Type 1454-A voltage divider. This cancellation is accomplished at zero dc field when the superconducting specimen is diamagnetic to the ac field.

The resulting difference signal, which represents just the flux passing through the specimen, is observed at various dc fields by two methods. First, it is amplified, integrated or differentiated, and observed on an oscilloscope using either a Tektronix type-O plug-in unit or a Dymec 2460 A operational amplifier. When operating in the integration mode, a 1-cps low-frequency roll-off filter was used to eliminate zero drift. To allow the observation of phase shifts, the oscilloscope traces are triggered by the voltage developed across the drive coils. In the second method of observation, the signal is amplified with a Princeton Applied Research model CR-4 low-noise amplifier and then detected with a Princeton Applied Research model JB-6 two-phase lock-in amplifier measuring both the in-phase and quadrature components at the fundamental frequency. For some measurements the y axis of the x-y recorder is excited by the in-phase or quadrature recorder output of the JB-6. Using the lock-in amplifier system the response of the superconductor to ac fields of the order of 1 mOe in amplitude could be measured effectively.

Static magnetization curves were obtained by direct electronic integration using the methods described by Fietz[26] in the same Dewar and magnet system used for the ac measurements.

B. Sample Preparation

The measurements reported here were taken on cylindrical samples of Pb–2.3 wt % In alloy.[27] The samples, 30–60 mils in diameter, were extruded from a slug of the alloy prepared from 99.999+ starting materials, cut to a length of approximately 2 in., and each placed in a bent clean Pyrex glass tube which was then evacuated to $\approx 1\times10^{-7}$ mm Hg and sealed off with residual pressure less than 6×10^{-7} mm Hg. One end of the tube containing the specimen was placed in an annealing furnace while the opposite end was immersed in liquid nitrogen to serve as a trap during the anneal. The specimens were annealed in this manner for about 2 weeks at a temperature within 5–10°C of the melting point. The samples were kept in the evacuated tubes with liquid-nitrogen trapping until measurement.

Prepurified nitrogen gas was flushed over the sample during the transfer from the evacuated tube to the measuring coil, keeping the exposure of the surface to room atmosphere to less than 1 min. Between measure-

[26] W. A. Fietz, Rev. Sci. Instr. 36, 1621 (1965).

[27] Analysis of the samples was carried out for us by the Analytical Facility of the Materials Science Center at Cornell, supported by the Advanced Research Projects Agency.

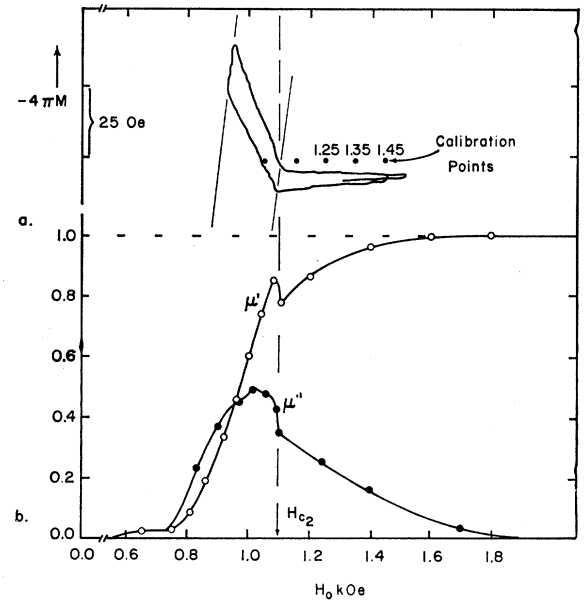

FIG. 4. H_{c2} is determined from both dc and ac magnetization measurements. In (a), an experimental dc loop close to H_{c2}. The small closure failure is due to a slight drift in the electronic integrator. H_{c2} is taken as the midpoint of the diamagnetic line joining the breaks in the curve. In (b) the corresponding deviation in the ac curve is shown.

ments, the samples were kept in liquid nitrogen to prevent deterioration of the surface.

C. Specimen Characteristics

In general, H_{c2} should be determined by dc magnetization curves. Figure 4(a) shows an expanded experimental curve in the region close to H_{c2} and shows a break in both the increasing and decreasing curves. The center of the diamagnetic line joining the two breaks is taken as H_{c2}.

An alternative measure of H_{c2} which we have used is the point at which the discontinuity in slope of μ' and μ'' as a function of H_0 occurs. This is illustrated in Fig. 4(b). Table I shows comparisons of values of H_{c2} determined by both methods and shows essential agreement. The values determined by the ac method are perhaps 1% higher.

The normal-state resistivity of the samples discussed here was found to be 3.2–3.4 $\mu\Omega$ cm. At the highest frequency we wish to consider, 500 cps, this leads to a normal-state penetration depth $\delta_n=0.5$ cm. For specimens used in these experiments, normal-state skin-effect calculations[11] show that $\mu'=0.9998$ and $\mu''=0.0112$. Hence, the specimens are transparent to the ac field when normal.

TABLE I. Comparison of values of H_{c2} determined by both dc and ac methods. The field values in this table have been increased by ½% to allow for the discrepancy between the field-probe position and the specimen position.

Specimen	dc (Oe)	ac (Oe)
Pb 2B−2	1095±5	1100±10
Pb 2B−1	1085±5	1090±10
Pb 2C−2	1093±5	1100±10
Pb 2C−2	1095±5	1105±10
Pb 2D−1	1100±5	1110±10

The value of the G-L parameter κ has been determined from the normal-state resistivity using the Gor'kov relation in the form proposed by Goodman,[28] and taking[5] $\kappa_0=0.38$, and $\gamma=1700$ erg/cm^3°K,[2] the value for pure lead.[29] From this value, $\kappa=1.43$, and the measured value of H_{c2}, we find the thermodynamic critical field $H_c=545$ Oe, in agreement with the value obtained for pure Pb[29] (see also Livingston[30]). The value of κ is consistent with the value determined from the slope of the dc magnetization curve at H_{c2}.[31]

4. RESULTS

A. Wave Form

Figure 5(a) shows superimposed wave forms observed at 50 cps resulting from an applied sinusoidal ac field 12.1 Oe in amplitude at three different dc fields. The signal represents $d\Phi/dt$, where $\Phi(t)$ is the flux through the specimen. When the dc field is above H_{c3}, the specimen is normal and an undistorted sine wave is obtained for $d\Phi/dt$. The distorted sine waves correspond to dc fields between H_{c2} and H_{c3} with the distortion increasing as the dc field is decreased Figure 5(b) shows traces of $\Phi(t)$ obtained by electronic integration of the pickup signal. Two traces are shown corresponding to the highest and lowest dc fields used in Fig. 5(a).

Since the samples are normal, the undistorted traces shown in Figs. 5(a) and 5(b) represent the applied ac field $h(t)$. The thickness of the superconducting surface sheath is very small compared to the radius of the specimen and the internal field may be regarded as constant in space for all dc field values above H_{c2}. Thus $\Phi(t)=Ab(t)$, where A is the cross-sectional area of the sample and $b(t)$ is the internal field.

At low frequency, as seen from the $d\Phi/dt=Adb/dt$ wave forms shown in Fig. 5(a), the transition can be characterized by three regions: (1) a region in which $db/dt=0$, (2) a transition region, and (3) a region in which $db/dt=dh/dt$. Region 1 starts abruptly when dh/dt changes sign and corresponds to current being developed in the surface sheath screening the interior completely from the change in the applied field. When the current reaches a critical value, which we operationally defined as the critical current J_c, the ac field begins

[28] B. B. Goodman, IBM J. Res. Develop. **6**, 63 (1962).
[29] B. L. Decker, D. E. Mapother, and R. W. Shaw, Phys. Rev. **112**, 1888 (1958); B. J. C. Van der Hoeven, Jr., and P. H. Keesom, *ibid.* **137**, A103 (1965).
[30] J. D. Livingston, Phys. Rev. **129**, 1943 (1963).
[31] W. H. Kleiner, L. M. Roth, and S. H. Autler, Phys. Rev. **133**, A1226 (1964); G. Eilenberger, Z. Physik **180**, 32 (1964).

to penetrate into the interior of the specimen, marking the start of the transition region. At this point the internal field lags the applied field by an amount $h_c=4\pi J_c/c$. Throughout the transition region, the current continues to increase, reaching a maximum value, which we denote as J_s, at the onset of region 3. Since throughout the rest of the half-cycle $db/dt=dh/dt$, the circulating current in the surface sheath remains constant and equal to J_s and the internal field lags the applied field by $h_s=4\pi J_s/c$. The current induced in the surface sheath is diamagnetic in the positive half-cycle of the ac field and paramagnetic in the negative half-cycle. It is apparent from these observations that the specimen traverses a hysteresis loop during the course of the cycle and examples are shown in Fig. 5(c). At low frequency, the hysteresis loop is quasistatic, with the initial penetration of the ac field occurring at h_c but the over-all width of the loop determined by h_s. Both h_c and h_s are functions of the dc field applied to the sample.

B. Model

The form of the observed wave form suggests directly a simple model to be used for quantitative discussion. This is to assume only one critical current J_m and the corresponding critical ac field amplitude $h_m=4\pi J_m/c$. We sketch the model wave form for $d\Phi/dt$ and $\Phi(t)$ in comparison with the observed wave form in Figs. 6(a) and 6(b). We also illustrate in Fig. 6(c) the distinction between the model hysteresis loop and the observed hysteresis loop. Note that for ac field amplitudes h_0 close to h_c, an appropriate value for h_m is h_c, whereas for $h_0\gg h_c$, h_m should be h_s (see also Sec. 4C). The numbers 1–6 correspond to equivalent points in the cycle. It will be seen that in regions $2\rightarrow 3$ and $4\rightarrow 5$, $b(t)=h(t)\pm h_m$, as was suggested by the observations. It is in this respect that the model proposed here differs from that proposed in detail by Fink.[14] Fink approximated the wave form in the regions $2\rightarrow 3$ and $4\rightarrow 5$ with a linear time dependence. The model critical field h_m is considered to be a function of the dc field.

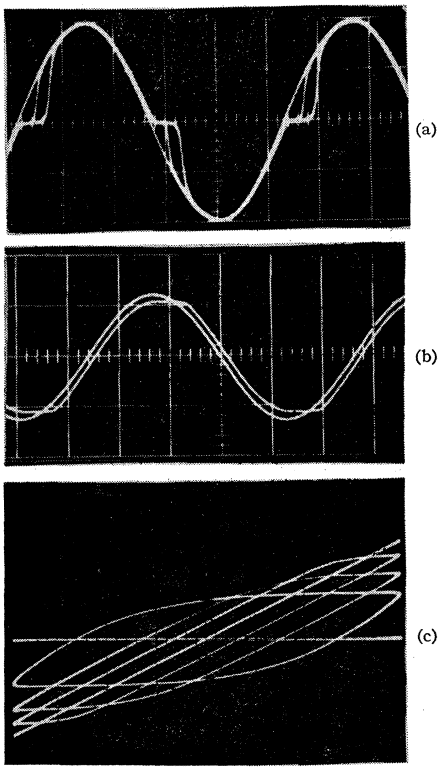

FIG. 5. Experimental observations of (a) db/dt, (b) $b(t)$, and (c) the induction loop for Pb–2.3 wt% In samples at a frequency of 50 cps and an ac field amplitude of 12.1 Oe. The sine curves in (a) and (b) and the straight line in (c) correspond to $H_0>H_{c3}$, whereas the distorted curves [(a) and (b)] and the loops (c) correspond to $H_{c3}>H_0$.

Fourier analysis of the model wave form yields an expression of the form

$$b(t)=h_0\sum_{n=1}^{\infty}(\mu_n'\cos n\omega t+\mu_n''\sin n\omega t), \tag{6}$$

where we assume $h(t)=h_0\cos\omega t$. If $h_0<h_m$, $b(t)=0$. If $h_0\geq h_m$, the real and imaginary parts of the ac permeability at the fundamental frequency are given by

$$\mu_1'=(2\pi-2\theta+\sin 2\theta)/2\pi,$$
$$\mu_1''=\frac{\sin^2\theta}{\pi}=\frac{4}{\pi}\frac{h_m}{h_0}\left[1-\left(\frac{h_m}{h_0}\right)\right], \tag{7}$$

where

$$\theta=2\sin^{-1}(h_m/h_0)^{1/2}.$$

The permeabilities at the higher harmonics are given for $h_0\geq h_m$ by

$$\mu_n'=\frac{1}{\pi n}\left\{\frac{\sin(n+1)\theta}{n+1}-\frac{\sin(n-1)\theta}{n-1}\right\},$$
$$\mu_n''=\frac{1}{\pi n}\left\{\frac{1-\cos(n+1)\theta}{n+1}-\frac{1-\cos(n-1)\theta}{n-1}\right\}, \tag{8}$$

where only odd harmonics are present and $\mu_n''\lesssim(\pi n^2)^{-1}$. If $h_0\gg h_m$, then $\theta\sim 2(h_m/h_0)^{1/2}\ll 1$ and μ_1' approaches its normal-state value of 1, while all the other permeabilities approach zero. It is evident that $b_1''=\mu_1''h_0$ saturates at a value of $4h_m/\pi$ at large h_0. These limits for μ_1' and μ_1'' are quite different from those of Fink's linearized approximation to the wave form.

We have assumed in the above development that $\mu_1'=1$ and $\mu_1''=0$ for the specimen in the normal state. As mentioned earlier, this is a good approximation for our specimens at the frequencies studied. However, if higher frequencies were used the normal skin effect would have to be taken into account. This may be done by simply assuming the interior of the sample is always normal and sees, as the applied field, the $b(t)$ calculated above. This approach assumes that the response of

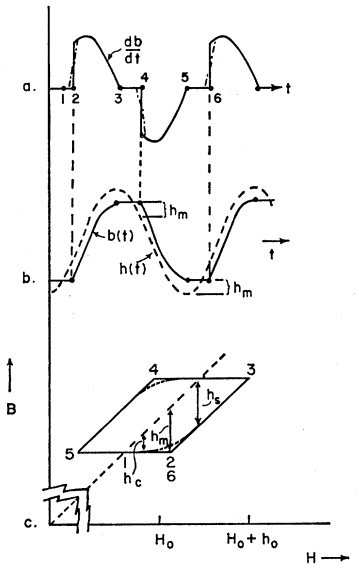

FIG. 6. The model wave form for (a) db/dt and (b) $b(t)$ is shown together with (c) the corresponding induction loop. In (a) and (c) the relationship to the experimental curves [Fig. (5)] is shown.

the surface sheath is frequency-independent, which is not necessarily true, as we will discuss presently. Nevertheless, this approach could be useful when considering samples with low resistivities and large radii at relatively low frequencies. If we denote the total permeability at the nth harmonic as $\mu_n'(\omega)$, $\mu_n''(\omega)$, and denote the normal-state permeability of the sample at frequency $n\omega$ by $\mu_{\text{norm}}'(n\omega)$, $\mu_{\text{norm}}''(n\omega)$, then we obtain

$$\begin{aligned}\mu_n'(\omega)&=\mu_n'\mu_{\text{norm}}'(n\omega)-\mu_n''\mu_{\text{norm}}''(n\omega),\\ \mu_n''(\omega)&=\mu_n'\mu_{\text{norm}}''(n\omega)+\mu_n''\mu_{\text{norm}}'(n\omega).\end{aligned}\tag{9}$$

Throughout the remainder of the paper, however, we shall be concerned only with the fundamental components b_1', b_1'', μ_1' and μ_1'' and the subscript will be dropped.

C. Constant dc Field Measurements

Theory suggests that the critical current (possibly J_c in the present experiments) is a monotonic function of the dc field. This fact, together with the model described above, implies that h_c can be found most simply by keeping the dc field (and hence h_c) constant and finding b' and b'' as a function of h_0. Figure 7(a) shows a typical set of x-y recorder traces of b' and b'' as a function of h_0 for several different values of the dc field H_0. Above H_{c3}, $b'=h_0$ while $b''=0$, reflecting the fact that the normal skin depth is much larger than the radius of the sample. Below H_{c3}, b' and b'' show behavior very close to that predicted by Eq. (7). The predicted saturation of b'' is evident. Figure 7(b) shows similar data reduced by h_c in each case for three different values of H_0. It should be noted that the plots superimpose closely, indicating that the curves are determined by one parameter, e.g., h_c, which is a function of H_0. Also shown are the curves predicted by Eq. (7) together with those of Fink's model. We have fitted the curves with $h_m=h_c$, where h_c is the field at which flux first enters. The major discrepancy between the data and the model lies in the saturation value of b'' and arises from neglect of the finite width of the transition region mentioned earlier. In general, the shielded field h_s is experimentally larger than h_c. Since $h(t)=h_0\cos\omega t$, all of the power absorbed per cycle is related to the fundamental component μ'' by $\Delta E=\frac{1}{4}h_0^2\mu''$ and may be equated to the area enclosed by the B-H loop divided by 4π. The over-all width of the B-H loop is given by h_s and thus for h_0/h_s large, b'' should be determined by h_s rather than h_c.

D. Constant ac Field Measurements

Figure 8 shows data taken in the conventional manner,[5–10] showing μ' and $\mu''(=4\pi\chi'')$ plotted as a function of H_0 at four different ac field amplitudes. The detailed shape of the curves is difficult to describe in terms of the model since it depends on the functional

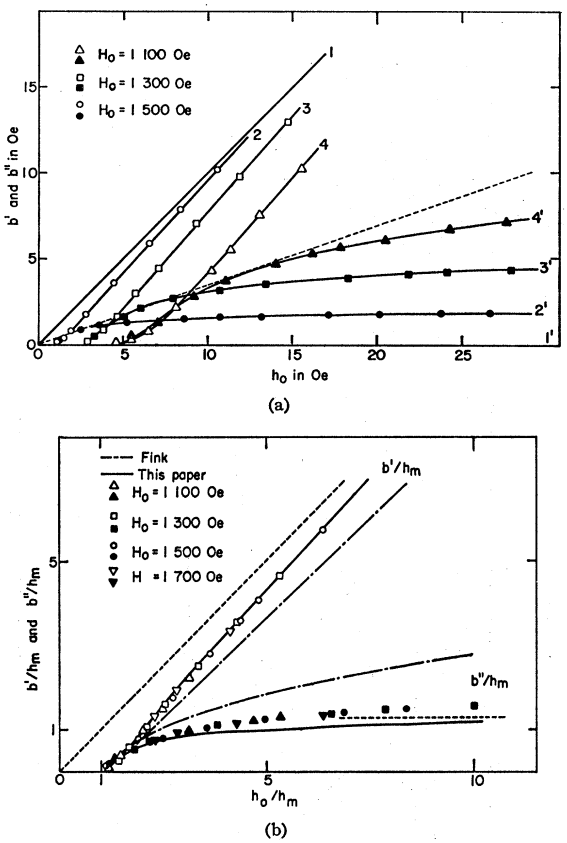

FIG. 7. (a) Unreduced data for b' (open symbols) and b'' (solid symbols) as a function of h_0 at constant H_0. Curves 1 refer to $H_0>H_{c3}$, whereas curves 2, 3, and 4 are for $H_{c3}>H_0>H_{c2}$. Accuracy is better than the size of spots. (b) Data for b' and b'' reduced by h_c lie on a universal curve. Four values of H_0 covering the full range $H_{c3}>H_0>H_{c2}$ are utilized. Also shown are the predictions of Fink's model and the model put forward in this paper. The dashed line at 45° represents the normal-state response for b' and the horizontal dashed line the saturation value of this model.

TABLE II. Comparison of experiments with predictions of various models.

	Uniform σ_n	Sheath σ bulk σ_n	Fink model	Our model	Expt. (50 cps)
μ'' at max	0.377	0.5	0.425	$0.32(=\pi^{-1})$	0.34
μ' at max	0.617	0.5	0.53	0.5	0.52
Condition	$a(4\pi\sigma_n\omega/c^2)^{\frac{1}{2}}=2.51$	$ad(2\pi\sigma\omega/c^2)=1$	$h_0=2.6h_c$	$h_0=2h_m$	

dependence of h_m on H_0. It is easily seen from Eq. (7) that the requirement $d\mu''/dh_m=0$ predicts a maximum in μ'' when $h_m/h_0=\frac{1}{2}$. The height of the peak is $\mu_{\max}''=1/\pi$, while $\mu'=\frac{1}{2}$ at the position of the maximum. These values compare favorably with the observed values. It should be pointed out, however, that this form of plotting the data is not nearly as sensitive to the type of model used as are plots of μ' and μ'' versus h_0 at fixed H_0. Table II shows that all the models, including those which are linear in h_0, predict a peak in μ'' of about the same magnitude and at nearly the same value of μ'. Consequently, all are not in bad disagreement with experiment in this respect. We should note that all the models, including the one proposed here based on the observed wave form, predict the height and position of the peak relative to μ' to be independent of h_0. This is not always observed to be the case, as is evidenced most strongly by the data of Van Engelen *et al.*[9] However, the strongest disagreement seems always to come in specimens which also show anomalously high ratios of H_{c3}/H_{c2} and may be related to a poor surface condition.

In the case of the measurements described in the previous section, the straight-line envelope of the b'' data [see Fig. 7(a)] corresponds to the constant value of the peak height discussed here. Thus, in this model, db''/dh_0 evaluated at $h_0=2h_m$, the point corresponding to the peak height, is $\mu_{\max}''=0.32$ and experimentally this is ≈ 0.345, which is reasonably close. The latter value is in excellent agreement with the experimental value for the peak of 0.34. This reflects the closeness with which the data can be superimposed [see Fig. 7(b)]. If $b''=h_0f(h_m/h_0)$, where f is now a general function with a maximum, then $\mu_{\max}''$ will be the maximum value of f and the envelope of b'' in curves of the type shown in Fig. 7(b) will be $\mu_{\max}''h_0$. Thus, although we do not have quite the right form for f, the agreement of $\mu_{\max}''$ determined from the peak with that determined from the slope of the envelope confirms the deduction that only one parameter dependent on the dc field is needed to describe the situation. In the case of the data reported by Van Engelen *et al.*, this may not be the situation.

The peak rises steeply on the low-field side of the

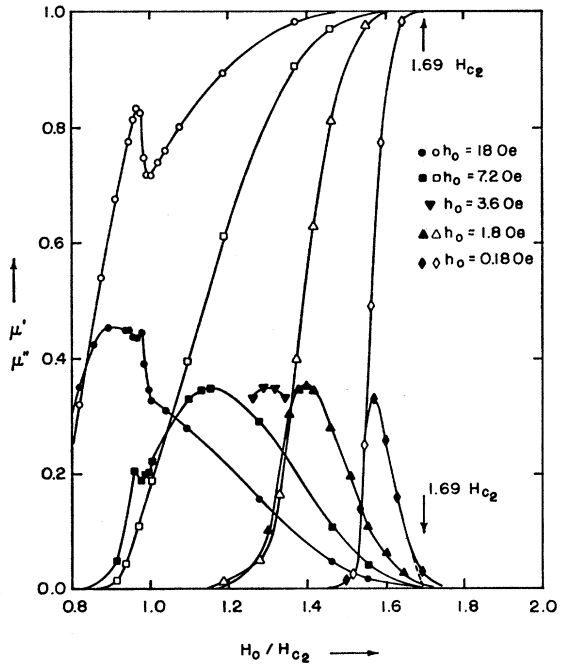

FIG. 8. Conventional plots of μ' and μ'' as a function of H_0/H_{c2} for five different ac field amplitudes.

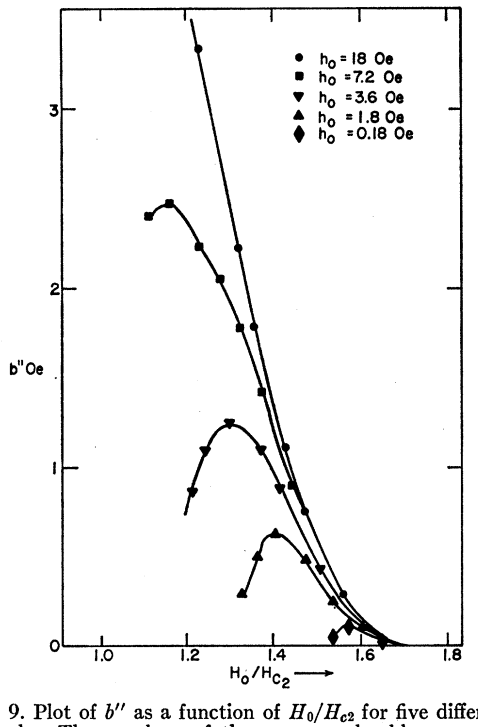

FIG. 9. Plot of b'' as a function of H_0/H_{c2} for five different ac amplitudes. The envelope of these curves should represent the function $h_s(H_0)$.

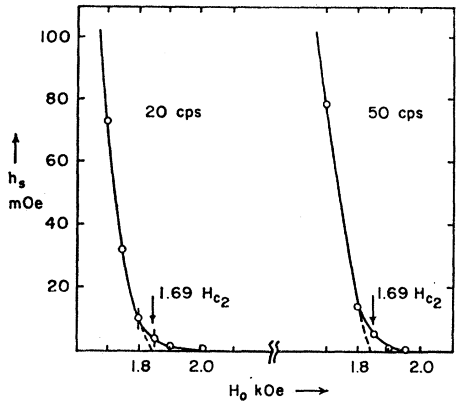

FIG. 10. $h_s(H_0)$ curves shown at high sensitivity to indicate a possible tail above $H_{c3}=1.69\ H_{c2}$. The accuracy of the values is indicated in the error bars on the 20-cps curve.

maximum corresponding to the sharp increase in μ'' for h_0 just greater than h_c, as seen in Fig. 8. The shallow high-field decline reflects the decrease in h_s as H_0 approaches H_{c3}. This is illustrated in Fig. 9, which shows b'' as a function of H_0 for four different h_0. It will be seen that the high-field tails of the b'' curves tend to an envelope identified as $4h_s(H_0)/\pi$. It is apparent that very high values of h_0 relative to h_s are needed to make b'' saturate.

E. Values of H_{c3}

By looking at values of $h_s(H_0)$ with high sensitivity close to H_{c3}, curves of the form shown in Fig. 10 are obtained. Taking 1980 Oe as H_{c3}, i.e., the field at which $h_s=0$, and $H_{c2}=1093$ Oe, gives $H_{c3}/H_{c2}=1.81$. However, the curves can be plausibly extrapolated as indi-indicated to $H_{c3}=1850$ Oe, corresponding to a ratio $H_{c3}/H_{c2}=1.69$.[3] We suspect that the tail is anomalous,[32] although we have no direct proof. A similar tail is sketched in Fig. 8. Other evidence of an anomalous effect is that for very small amplitude ac fields at H_0 close to H_{c3}, the magnitude of the peak begins to drop from the constant value of 0.34 (see also Sec. 4F).

F. Orientation Dependence

Both H_{c3}[33] and the values of J_s are orientation-dependent. Figure 11 shows a plot of $J_s(\nu)/J_s(0)$ at several different values of H_0, where ν is the angle between the applied field and the axis of the specimen. The ac field is always applied along the axis of the specimen. Also shown is $H_{c3}(\nu)/H_{c3}(0)$. It will be noted that J_s is in general much more dependent on ν than H_{c3}. As pointed out by Bertman and Strongin,[33] this is to be expected since J_s may go to zero while H_{c3} may vary only from H_{c2} to 1.7 H_{c2}.

For angles ν close to alignment, it is found that J_s has a slightly stronger angular dependence for H_0 near H_{c2} than near H_{c3}. In the present example the two curves cross at angles further away from full alignment. This is due to the angular dependence of H_{c3}, since H_{c3} becomes 1775 G at an angle slightly greater than 4° in this sample. The finite but small currrent observed at 5° is due to the tail discussed above (Sec. 4E). From these observations, we find it necessary to align our specimens to within $\pm\frac{1}{4}°$ or better and to carry out the alignment with the dc field close to H_{c2}. We note that if the sample is misaligned by 1°, the critical current can drop by as much as 40%.

G. Critical Currents

From the experiments described above, we can determine h_c to compare with the theories of Abrikosov,[18] Park,[19,20] and Fink and Barnes.[21] In the present case, h_c is determined by the intersection of a straight line $b'=\frac{1}{2}h_0$ with the experimentally determined curve. In terms of the model, this point corresponds to the maximum in $\mu''(H_0)$ at constant h_0, and b' is equal to h_c at this point. Thus, these data can be compared with others, both in the literature and in the present study, determined from the maximum in $\mu''(H_0)$. Experimentally, however, the numbers are roughly 30% higher than the critical currents found from the first detectable field penetration as determined by rather subjective criteria.

Figure 12 shows data for J_c for two Pb–2% In samples obtained in this fashion. The samples were given identical treatments separately so that the data are a

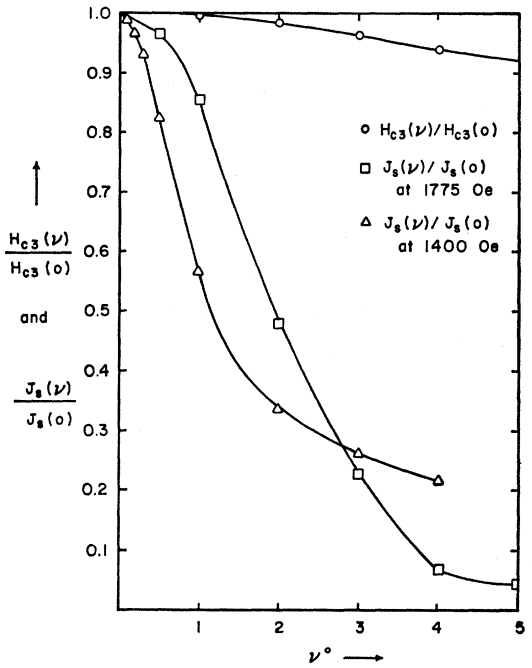

FIG. 11. The orientation dependence of H_{c3} and J_s.

[32] P. R. Doidge, K. Sik-Hung, and D. R. Tilley, Phil. Mag. 13, 795 (1966).
[33] B. Bertman and M. Strongin, Phys. Rev. 147, A268 (1966).

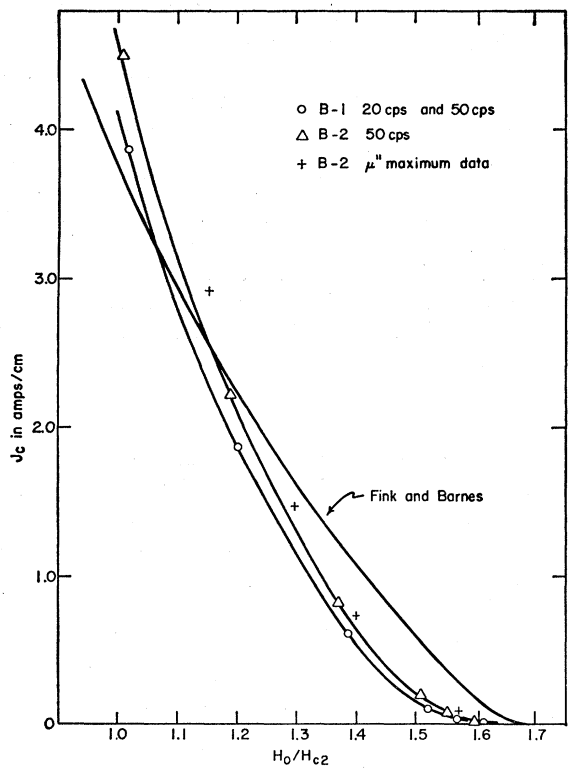

FIG. 12. Comparison of the critical currents for two specimens with the theoretical predictions of Fink and Barnes.

measure of the reproducibility of samples. In addition, data obtained using the maximum in $\mu''(H_0)$ as indicated in Sec. 4D are shown. The agreement is reasonable. Also shown is the theoretical prediction of Fink and Barnes which comes closest in order of magnitude. The discrepancy is largest close to H_{c3}.

The same data are compared with the theoretical predictions of Abrikosov[18] (A) and the refinement due to Park[19] (PI) and also Park's[20] (PII) refinement of Fink and Barnes's predictions in a logarithmic plot in Fig. 13 as a function of $(1-H_0/H_{c3})$, where we have taken $H_{c3}=1.7H_{c2}$. This plot emphasizes the discrepancy close to H_{c3}. It is plain that agreement occurs only close to H_{c2} and that the variation with H_0 is much steeper than predicted. If we take $J_c \propto (1-H_0/H_{c3})^n$, then n is approximately 3 and can be compared with the transport-current data of Bellau,[34] who found values of n ranging from 2 to 5 and the theoretical prediction[18] of $\frac{3}{2}$. The data are comparable with other data in the literature.[33–35]

H. The Nature of the Transition

The difference between h_s and h_c, as determined from the permeability measurements discussed in Sec. 4C, shows that the ideal model put forward in Sec. 4B is not entirely realized in practice. Typically, $h_s \approx 2h_c$ and this makes any careful quantitative comparison with the various theories difficult. Deviations from the ideal-model transition may conveniently be separated into two categories: frequency-independent effects and frequency-dependent effects. The frequency-independent effects will be discussed first.

Frequency-Independent Effects

Figure 14 shows oscilloscope traces of db/dt observed in response to a sinusoidal ac field taken with an expanded sweep rate to reveal any structure in the transition. The specimen was a Pb–2 wt% In cylinder 32 mils in diameter. All the transitions are shown with $H_0/H_{c2}=1.1$, $h_0=12.1$ Oe and at a frequency of 50 cps, but each with the axis of the sample at a slightly different angle to the dc field direction. Lowering the

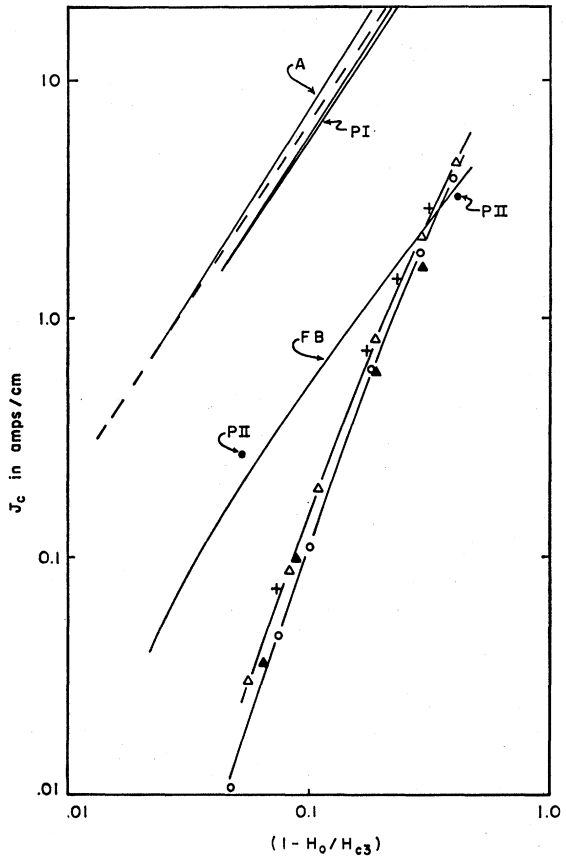

FIG. 13. Logarithmic plot of the same data as in Fig. 12 for comparison with Abrikosov (Ref. 18) (A), Park (Ref. 19) (PI), Fink and Barnes (Ref. 21) (FB), and Park (Ref. 20) (PII). Also shown (closed triangles) are data taken using a short drive coil to supply the ac field. In this case the ends of the specimen were outside the ac field and hence could not act as nucleation sites for transitions. From the agreement it is concluded that end effects are not playing an important role in determining the critical current. (The suggestion that end effects might be important was made to us by Professor W. F. Vinen.)

[34] R. V. Bellau, Phys. Letters **20**, 13 (1966).
[35] P. S. Swartz and H. R. Hart, Jr., Phys. Rev. **137**, A818 (1965).

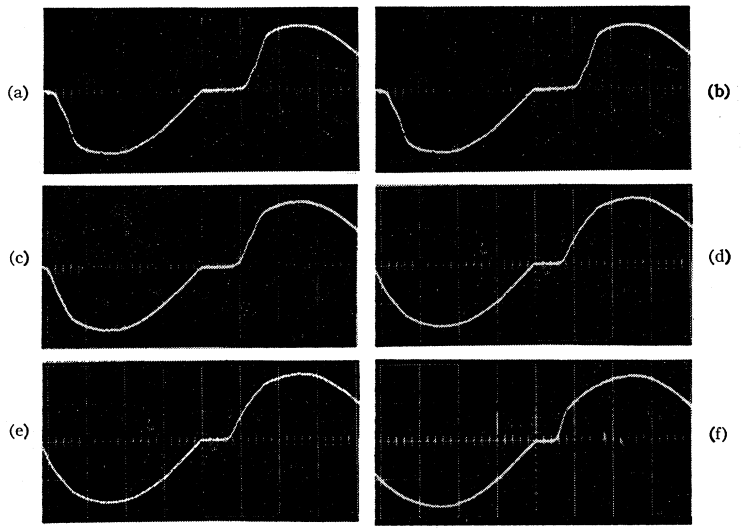

FIG. 14. Oscilloscope traces of db/dt as a function of misorientation with respect to the applied field: (a) $\nu=0°$, (b) $-\frac{1}{2}°$, (c) $+\frac{1}{2}°$, (d) $+1°$, (e) $-1°$, (f) $-2°$.

frequency below 50 cps did not change the structure of the transition appreciably in this case. Figure 14(a) was taken with the dc field directed along the axis of the specimen determined by maximizing J_s, as described previously. It will be noted that the transition shows considerable structure, suggesting that there are many different critical currents, three of which are particularly prominent, acting in the area of the specimen contained within the measuring coil. Figure 14(b) shows the same transition, but with the field misaligned by $-\frac{1}{2}°$. (The + and − directions are defined arbitrarily.) It will be seen that the structure has changed considerably from that shown in Fig. 14(a). Figures 14(c), 14(d), 14(e), and 14(f) correspond to deviations from alignment of $+\frac{1}{2}°$, $+1°$, $-1°$, and $-2°$, respectively. It is to be noted that a slight misalignment changes the transition considerably. In general, misalignment tends to smooth out the transition.

It may be concluded from these photographs that part, if not all, of the cause for the finite width of the transition region at low frequency is a range of critical currents. This could be caused, for example, by small irregularities on the surface forcing regions of the surface into misalignment with the dc field, resulting in local variations of the critical current which the sheath can support. Changing the alignment slightly brings different regions of the surface parallel to the dc field and hence changes the structure, as well as the absolute magnitude, of the observed transition. The structure within the transition is observed to be dependent on the magnitude of the dc field, although the over-all width of the transition is relatively unchanged. It should be pointed out that, although chemical polish may increase h_c considerably,[22] it does not necessarily make the transition any sharper.

Frequency-Dependent Effects

Figure 15 shows the frequency dependence of the same transition discussed above. Traces of db/dt are again shown with the sample aligned with the dc field. Also shown for reference are traces of the applied field obtained by increasing the dc field above H_{c3}. Figure 15(a) shows the response to a 50 cps ac field, while Fig. 15(b) was taken at 500 cps. The time constant of the measuring coil with the specimen normal was measured by observing the response to a triangular ac field with the dc field above H_{c3}. This gave a time constant of about 20 μsec, which is $\frac{1}{10}$ major division on the oscilloscope trace taken at 500 cps and does not explain the shift of the wave form, although it could account for part of the smoothing of the transition.

Figure 16 shows the frequency dependence of a more ideal transition. The sample is specimen B-1, for which the critical-current data are shown in Figs. 12 and 13. Figures 16(a) and 16(b) show the transition at 20 and 500 cps, respectively. The transitions are shown with $H_0/H_{c2}=1.27$ and $h_0=12.1$ Oe. It will be seen that the lower critical current J_c, i.e., the point marking

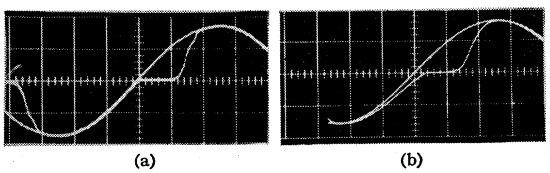

FIG. 15. Frequency dependence of db/dt wave form for the same specimen illustrated in Fig. 14: (a) 50 cps, (b) 500 cps.

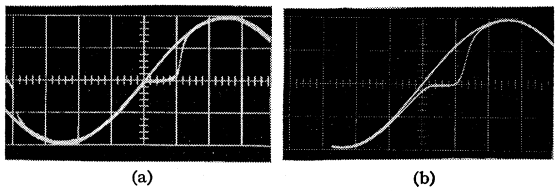

FIG. 16. Frequency dependence of db/dt wave form for a more ideal specimen ($B-1$): (a) 50 cps, (b) 500 cps.

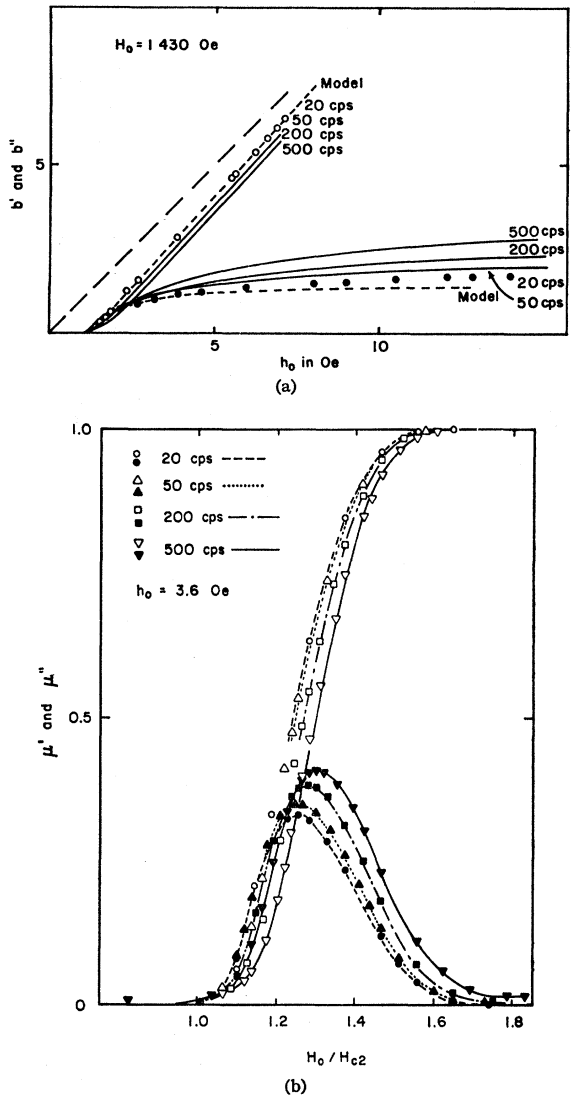

FIG. 17. (a) Frequency dependence in plots of the type discussed in Sec. 4C. The b' plots for 20 and 50 cps closely superimpose on the model prediction. (b) Frequency dependence in permeability curves of the type discussed in Sec. 4D.

the onset of the transition region, is much less sensitive to frequency than is J_s. It is also evident from the figure that region 3 as defined in Sec. 4A for low frequencies, no longer has the property $db/dt = dh/dt$. At higher frequencies db/dt gradually starts to lag dh/dt with the lag becoming more pronounced as dh/dt approaches and goes through zero. This implies that the shielding current is not constant throughout this region, as was assumed in the ideal model. In fact, at high frequencies, dh/dt and db/dt are of opposite sign for a short time after dh/dt goes through zero. Whereas at low frequency region 1 starts abruptly when dh/dt changes sign, at higher frequencies this region is approached more smoothly. If the frequency is not too high, one can still see a discontinuity in the slope of db/dt when db/dt finally reaches zero. [See, for example, Fig. 15(b)].

The frequency dependence is also evident in permeability measurements of the type discussed in Secs. 4C and 4D. Figure 17(a) shows recorder plots of b' as a function of h_0 taken on specimen B-1 at 20, 50, 200, and 500 cps. The curves were all plotted at the same dc field, $H_0/H_{c3}=1.3$. It will be seen that b'' curves are more sensitive to frequency effects than are the b' plots. The saturation value of b'' increases as the frequency, revealing the increase in h_s. The point at which the ac field starts to penetrate is again observed to be less dependent on frequency than is h_s. The same conclusion can be drawn from $\mu'(H_0)$ and $\mu''(H_0)$ curves shown in Fig. 17(b). It will be noted that the size of the peak has increased, reflecting the increase in h_s and that more power is therefore being absorbed corresponding to widening of the hysteresis loop.

5. DISCUSSION

A. Nature of the Transition

It is clear that the model described above (Secs. 4 A through 4 D) gives a very good description of the whole of the ac transition for "good" specimens at low frequencies. In general, only one parameter is needed to explain the dc field dependence. In terms of the free-energy diagram discussed earlier, the passage of the field around the hysteresis loop [Fig. 18(a)]

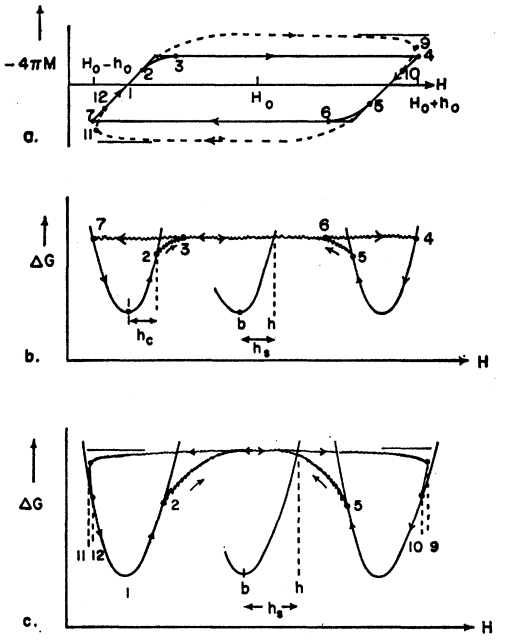

FIG. 18. (a) Magnetization loops for low (solid line) and high (broken line) frequencies. (b) Free-energy path taken by sample at low frequency. Transitions between parabolas are schematically shown by the jagged lines. The internal field b is given by the location of the minimum of the potential well in which the system is sitting at applied field h. Both h_c and h_s are shown. (c) Free-energy loop at a higher frequency.

in one cycle corresponds to the loop between two free-energy wells shown in Fig. 18(b). Thus at point 1 in the cycle, the internal field b and external field h are identical and the specimen is in a state at the bottom of the free-energy well. As h is increased, the specimen remains rigidly locked in this state until the point 2. Along the path from 1 to 2 there exist a multitude of lower energy states, but evidently no scattering mechanism exists whereby the sheath can relax into the lower levels.

The relaxation time eventually does become finite at 2 and transitions begin to occur. When transitions do occur, they may go via the normal state, but the final state is a lower lying superconducting state with a relatively small change Δn in n value. If the final state were the normal state, the currents in the sheath would collapse in about 10^{-6} sec for these samples, and this is not observed. Which state is the final state is governed by the kinetics of the process, and this process is not understood. This point of view is similar to that of Douglass,[36] who discusses persistent currents in a thin-walled superconducting cylinder.

The relaxation time does not match the rate at which the field increases until the point 3 is reached. From 3 to 4, the free energy stays constant while the specimen is undergoing transitions between states with $\Delta n>0$, corresponding to flux entry into the sample. This is region 3 of the observations and corresponds to the constant screening field h_s. If we note that $h_c \ll H_0$ in general, then Δg_n^0 [Eq. (3)] can be regarded as roughly a constant and, from Eq. (3), we find

$$\frac{d}{dt}(\Delta G)=\frac{h-b}{4\pi}\left(\frac{dh}{dt}-\frac{db}{dt}\right)=m\left(\frac{dh}{dt}-\frac{db}{dt}\right), \qquad (10)$$

where m is the magnetization. The first term in this expression we identify as the work being done on the sample by the applied field and the second term as the energy being dissipated by the sample as it changes states within the sheath ($db/dt \approx \pi R^2 \varphi_0 dn/dt$). Thus in region 3 these are equal, corresponding to $dh/dt=db/dt$, and the free energy stays at a constant level. When dh/dt changes sign, the system stays in the free-energy state it is in at that point until the point 5 is reached. During this, the magnetization has switched from diamagnetism to paramagnetism. The same procedure is followed on the reverse half of the cycle, only $\Delta n<0$ corresponding to flux expulsion from the sample.

Although we have preferred to discuss this in terms of relaxation times, it is clear that a nonlinear effective conductivity or voltage/current relation is an equally valid concept. However, in computing the consequences, linear-response theory, as used in the earlier models,[8,12] is not applicable. Parenthetically, it should be noted that the electric field calculated using the "extra" G-L equation[37] turns out in this case to be an equivalent field, corresponding to the relaxation mechanism and thus opposes the electric field generated by the changing applied magnetic field.

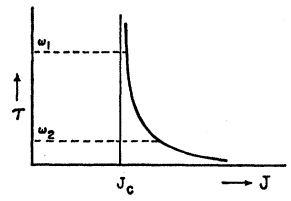

FIG. 19. Schematic representation of expected relaxation time for transitions between free-energy states.

B. Frequency Dependence

The corresponding free-energy loop at a higher frequency is shown in Fig. 18(c). It will be seen that db/dt no longer equals dh/dt as dh/dt approaches zero, but differs in a sense which allows the free energy to decrease, i.e., the free energy, or equivalently the shielding current, is relaxing to a lower value. This is also reflected in a rounding of the acute corners of the hysteresis loop [Fig. 18(a)]. Note that since h_s increases with frequency, the hysteresis loop is now wider and the level reached on the free-energy curve is higher.

To discuss the frequency dependence in detail, one would need a knowledge of the relaxation times involved. The expected form for the relaxation time is sketched in Fig. 19 as a function of the current carried in the sheath. Since J_c is given by the point at which the relaxation begins to decrease from infinity, we may expect this point to be only weakly frequency-dependent. However, J_s will be given by an appropriate balance between dh/dt, corresponding to acceleration of the superelectrons, and the rate of relaxation, corresponding to db/dt. At higher $dh/dt(=\omega h_0 \sin\omega t)$, i.e., higher ω, we may expect balance to be achieved with a shorter relaxation time and, therefore, higher J_s, as is observed. At the higher frequency ω_2, J_s is observed to drop as dh/dt approaches zero. This reflects a changing balance, i.e., the relaxation times become longer and on the lower part of the curve a significant change in J is obtained by a small change in the relaxation time. At a lower frequency ω_1, on the steeper portion of the curve, this is no longer true and although the relaxation time may change, the change in J is slight.

Since dh/dt is also dependent on h_0, it is likely that there may also be amplitude-dependent effects. As mentioned in Sec. 4 D, in many cases saturation of b_1'' is not completely achieved even at relatively low frequencies. The apparent slight increase of h_s with h_0 may be explained in terms of the same origin as the observed frequency dependence of h_s. It is easy to show from the model of Sec. 4 B that when $h_0 \gg h_m$,

[36] D. H. Douglass, Phys. Rev. 132, 513 (1963).

[37] P. W. Anderson, N. R. Werthamer, and J. S. Luttinger, Phys. Rev. 138, A1157 (1965).

$\theta=2(h_m/h_0)^{1/2}$ and that $|dh/dt|$ at the point in the cycle where the transition occurs is given by $|dh/dt|=2(h_0h_m)^{1/2}$. This is equivalent to an increase in frequency at fixed h_0 and thus results in the same observed increase in h_s.

C. Material Properties

We turn now from consideration of the transition itself to some characteristics of the specimens. As discussed in Sec. 4 H, the transition as observed directly in the wave form can be clean or jagged, showing several different critical currents depending on the specimen surface preparation, orientation with respect to the magnetic field, and frequency. The wave form shown in Fig. 5 was particularly clean and the specimen was chosen to illustrate the model for this reason. In this case $h_s=1.2h_c$ and the transition region was sharp. In other cases, h_s is larger and the transition is relatively broad and jagged. These observations suggest strongly that critical currents in these samples are determined by surface imperfections.

This conclusion is reinforced by the comparison of the critical-current data with the predictions of the various theories. For the specimens discussed in Sec. 4 F, great care had been taken in handling and preparation. Through this, and probably luck, a fairly clean transition had been obtained. Nevertheless, a comparison of the data with theory shows the data to be in general low in comparison with the lowest theoretical predictions (although the order of magnitude is right close to H_{c2}) and to show a much stronger dependence on H_0 than predicted. This implies either incorrect theories, or, alternatively, because of specimen surface problems, irrelevant theories. The latter seems preferable. An appealing speculation at this stage is that the initial critical current is governed by nucleation of a transition, whereas J_s, particularly at the higher frequencies, is governed by a limiting velocity with which a transition region propagates. The nucleation event will be strongly affected by surface defects.

6. CONCLUSIONS

From this work, we can draw the following conclusions:

(1) In well-annealed, carefully prepared samples, the ac transition in the superconducting sheath state can be described by a single-parameter model to a good approximation.

(2) By measuring b' and b'' as a function of h_0 at constant H_0 at low frequencies, well-defined accurate data can be obtained describing the transitions. Due to the use of ac techniques, this approach can be used with high accuracy and in regions of small critical currents with ease in comparison with dc magnetization measurements.

(3) Wave-form observations at low frequencies can be utilized to study the cleanness of the transition. From these and a comparison of critical currents with theoretical data, we conclude that it is likely that surface defects may still affect the transition.

(4) Energy is dissipated during the course of transitions between states by an unknown mechanism. Preliminary exploration of the frequency dependence suggests that interesting relaxation effects are occurring which may throw light on this situation.

ACKNOWLEDGMENTS

The authors gratefully acknowledge interesting conversations with Professor W. W. Webb, Professor J. W. Wilkins, Dr. B. W. Maxfield, M. R. Beasley, J. F. Emerson, W. A. Fietz, J. Gosselin, and P. J. Ortoleva and also profited from a discussion with Professor W. F. Vinen. Use of W. A. Fietz' dc magnetization apparatus and the assistance of J. Gosselin in taking some of the data and of Professor R. M. Cotts in calibration of the magnet are also acknowledged. Dr. H. J. Fink and Dr. M. Strongin kindly sent copies of manuscripts prior to publication. The work was supported by the U. S. Atomic Energy Commission. It also benefited from use of facilities supported by the Advanced Research Projects Agency.

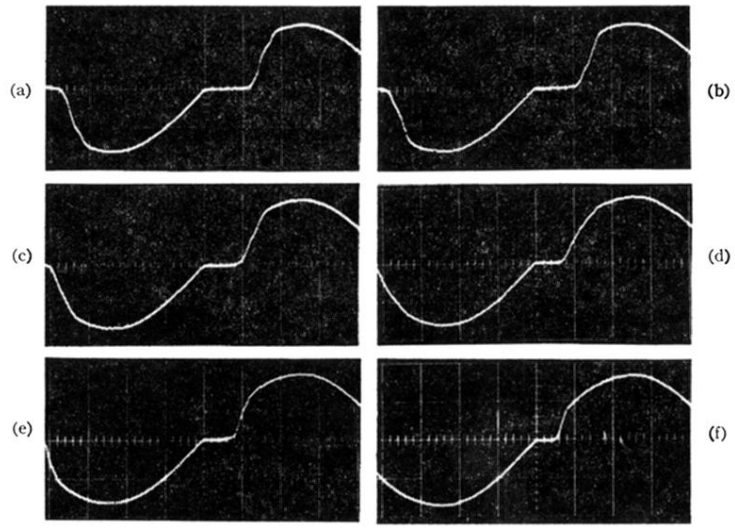

FIG. 14. Oscilloscope traces of db/dt as a function of misorientation with respect to the applied field: (a) $\nu=0°$, (b) $-\frac{1}{2}°$, (c) $+\frac{1}{2}°$, (d) $+1°$, (e) $-1°$, (f) $-2°$.

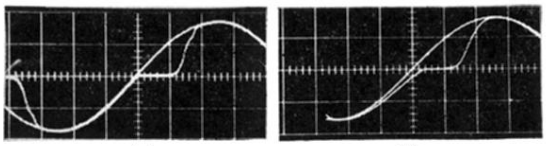

(a) (b)

FIG. 15. Frequency dependence of db/dt wave form for the same specimen illustrated in Fig. 14: (a) 50 cps, (b) 500 cps.

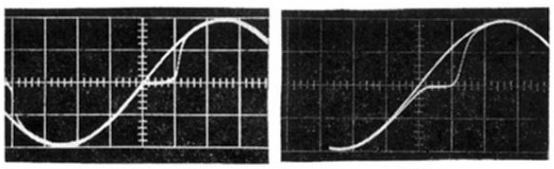

(a) (b)

FIG. 16. Frequency dependence of db/dt wave form for a more ideal specimen ($B-1$): (a) 50 cps, (b) 500 cps.

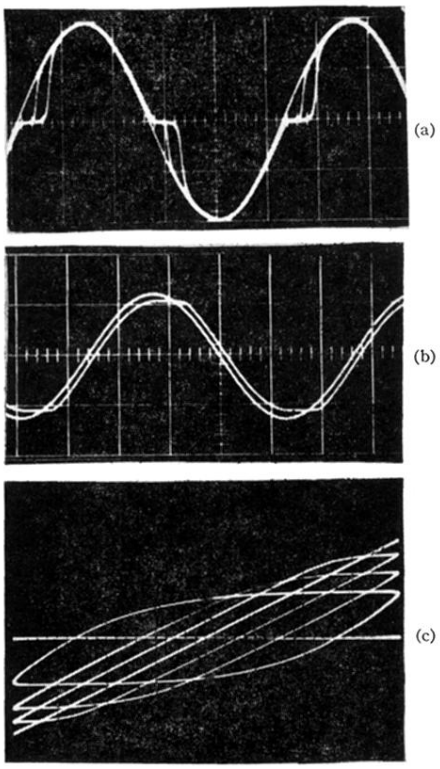

FIG. 5. Experimental observations of (a) db/dt, (b) $b(t)$, and (c) the induction loop for Pb–2.3 wt% In samples at a frequency of 50 cps and an ac field amplitude of 12.1 Oe. The sine curves in (a) and (b) and the straight line in (c) correspond to $H_0 > H_{c3}$, whereas the distorted curves [(a) and (b)] and the loops (c) correspond to $H_{c3} > H_0$.